APL Materials

Barrier materials for flexible bioelectronic implants with chronic stability—Current approaches and future directions

Cite as: APL Mater. 7, 050902 (2019); https://doi.org/10.1063/1.5094415
Submitted: 01 March 2019 . Accepted: 05 April 2019 . Published Online: 21 May 2019

Enming Song, Jinghua Li, and John A. Rogers

Barrier materials for flexible bioelectronic implants with chronic stability—Current approaches and future directions

Cite as: APL Mater. 7, 050902 (2019); doi: 10.1063/1.5094415
Submitted: 1 March 2019 • Accepted: 5 April 2019 •
Published Online: 21 May 2019

Enming Song,[1,2,a)] Jinghua Li,[2,3,a)] and John A. Rogers[1,2,3,4,b)]

AFFILIATIONS

[1]Center for Bio-Integrated Electronics, Northwestern University, Evanston, Illinois 60208, USA
[2]Frederick Seitz Materials Research Laboratory, Department of Materials Science and Engineering, University of Illinois at Urbana-Champaign, Urbana, Illinois 61801, USA
[3]Department of Materials Science and Engineering, Northwestern University, Evanston, Illinois 60208, USA
[4]Departments of Biomedical Engineering, Neurological Surgery, Chemistry, Mechanical Engineering, Electrical Engineering and Computer Science, Simpson Querrey Institute for Nano/biotechnology, Northwestern University, Evanston, Illinois 60208, USA

[a)]**Contributions:** E. Song and J. Li contributed equally to this work.
[b)]**Author to whom correspondence should be addressed:** jrogers@northwestern.edu.

ABSTRACT

Flexible, bio-integrated electronic systems have wide-ranging potential for use in biomedical research and clinical medicine, particularly as active implants with the ability to operate in a safe, stable fashion over extended periods of time. Here, the development of a thin, robust biofluid barriers that can simultaneously serve as long-lived sensing and/or actuating interfaces to biological systems represents a significant challenge. Requirements are for defect-free, biocompatible and impermeable materials that can be rendered in thin, flexible forms and integrated with targeted device platforms. This perspective summarizes various material strategies for this purpose, with a focus not only on properties and structures but also on their use in bioelectronic systems. The article begins with an overview of different classes of materials, including means to grow/synthesize/deposit, manipulate, and integrate them into test structures for permeability measurements and into systems for functional bio-interfaces. A comparative discussion of the most widely explored materials follows, with an emphasis on physically transferred layers of SiO_2 thermally grown on silicon wafers and on their use in the most sophisticated active, bendable electronic systems for electrophysiological mapping and stimulation. These advances suggest emerging capabilities in flexible bioelectronics implants as chronic implants with diagnostic and therapeutic function across a broad scope of applications in animal model studies and human healthcare.

INTRODUCTION

Advanced technologies that can establish long-lived, stable electronic interfaces to targeted biological systems are essential to the development of new classes of implantable devices with capabilities relevant to academic research and healthcare.[1–3] Flexible, high-performance electronic/optoelectronic systems with chronic operational stability in biofluids represent recent breakthroughs in this context.[4,5] Sophisticated, actively multiplexed platforms of this type are increasingly well established, with embodiments that range from thin sheets for electrophysiological mapping[6,7] on cardiac tissues to penetrating pins for neural recording in the brain.[8–10] These and other related systems are distinguished relative to technologies of the past by their compliant architectures and low bending stiffnesses as minimally invasive interfaces to curved, soft, and dynamic biological tissues, with electrical performance characteristics that can approach those of conventional wafer-based semiconductor devices.[11–16] Applications that involve long-term, safe operation in living organisms demand perfect isolation of the backplane electronics from surrounding biofluids to avoid leakage currents

into adjacent tissues and degradation of underlying devices.[17] The development of thin, defect-free layers of materials that can encapsulate such systems as robust biofluid barriers and, at the same time, as electrical interfaces to the surrounding biology represents a fundamental challenge, where operational timeframes may extend to the life of the patient (several decades or more).

Barrier layers must conform uniformly across the surfaces of flexible bioelectronic systems as seals against warm, circulating biofluids, with additional requirements for (1) low flexural rigidity, preferably less than that of the underlying electronics, to allow contacts with the moving, curved surfaces of targeted biological tissues, (2) defect-free structural properties with complete water, ion, and biomolecular impermeability over areas that can extend to many tens of square centimeters, (3) multidecade lifetimes at physiological conditions (i.e., temperature, pH, etc.), with engineering design goals for timeframes that are larger by an order of magnitude, (4) stable, low impedance bio-interfaces for sensing/stimulating the surrounding biology, and (5) excellent compatibility not only with the biology but also with a range of materials/devices in the underlying electronics. Previously reported materials, such as thin-film polymers and organic/inorganic multilayer stacks,[18,19] are of limited use primarily due to intrinsic limitations in water permeability and extrinsic effects associated with localized defects (arising from the growth process, i.e., pinholes, cracks, and grain boundaries), respectively. Although these approaches have some utility,[20–22] further progress is needed in most cases, especially for applications that involve most advanced, multichannel flexible electronic platforms where arrays of transistors provide capabilities in local amplification and multiplexed addressing.

The following summarizes the most effective flexible encapsulation strategies, beginning with some historical perspectives and requirements for various types of bio-integrated electronic platforms. Following discussions review various thin-film flexible materials for these purposes, with emphasis on physically transferred layers of SiO_2 thermally grown on device-grade silicon wafers (t-SiO_2). A combination of detailed studies, systematic permeability/immersion measurements, and comparative evaluations against many of most widely explored encapsulating films provides some context. Additional sections highlight the use of these materials with actively multiplexed bioelectronic systems to emphasize the capabilities and to describe opportunities for further progress. The results summarized here suggest that these encapsulation strategies will create opportunities for chronic operation of many types of flexible bioelectronic implants.

EMERGING CLASSES OF FLEXIBLE, BIO-INTEGRATED ELECTRONIC SYSTEMS

Encapsulation for conventional implants generally features rigid, thick (millimeter-scale) structures of metals, such as hermetic housings of titanium (Ti),[23] or of ceramics, such as cofired alumina-glass packages.[24,25] These robust enclosures isolate the electronics from surrounding biofluids, with lifetimes that can be measured in decades, as implants in humans. Unfortunately, the resulting systems are bulky and mechanically rigid and they do not allow for direct interfaces between the electronics and the curved, soft, time-dynamic surfaces of biological tissues. Specifically, these architectures separate the electronics from the biology in a way that dramatically limits the sophistication that is possible at the interface, with contacts that typically occur only at individual or small collections of hard-wired passive electrodes. Deep-brain stimulators, pacemakers, and other commercially available implants adopt these types of engineering designs.[26,27] An important future is one in which the electronics themselves, not just the electrodes, integrate directly with targeted tissues at scales, across areas and with levels of functionality that cannot be reproduced with existing paradigms. Flexible, high-performance electronic and optoelectronic platforms with chronic biocompatibility at the level of the mechanics, the geometry, and the constituent materials are of specific interest in this context.

Figure 1 outlines some of the most interesting and most recent implantable devices of this type in forms that include (a) filamentary probes, (b) open mesh networks, and (c) flexible sheets. More specifically, Fig. 1(a) highlights ultraflexible (a bending stiffnesses

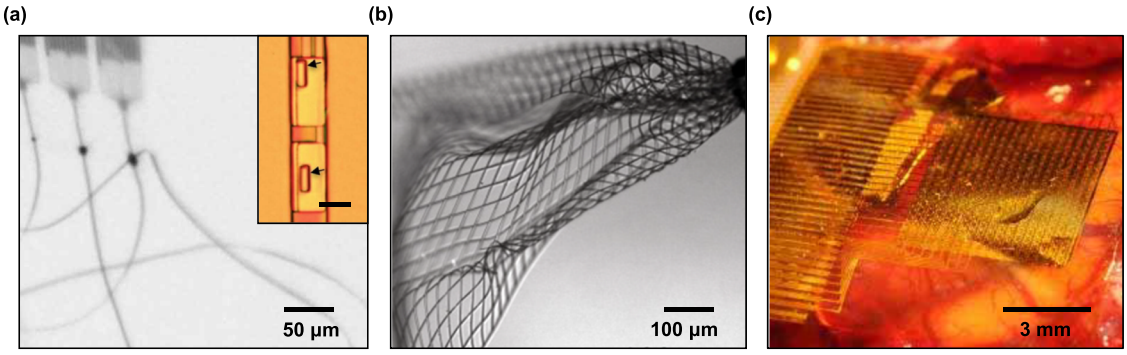

FIG. 1. Emerging classes of flexible, bio-integrated electronic systems. (a) Optical image of ultrathin (1.5 μm), narrow (10 μm) polymer (photodefinable epoxy, SU-8) needles, each of which supports four passively addressed electrodes (500 nm thick Au layers, an area of 200 μm^2). The inset shows an optical image of two such electrodes. The scale bar is 10 μm. Reproduced with permission from Luan *et al.*, Sci. Adv. **3**, e1601966 (2017). Copyright 2017 American Association for the Advancement of Science (AAAS). (b) Optical image of an open mesh platform for passive electrodes, injected into an aqueous solution through a syringe. Reproduced with permission from Liu *et al.*, Nat. Nanotechnol. **10**, 629 (2015). Copyright 2015 Springer Nature. (c) Photograph of a flexible sheet of actively multiplexed electronics placed on the cortical surface of a feline model. Reproduced with permission from Viventi *et al.*, Nat. Neurosci. **14**, 1599 (2011). Copyright 2011 Springer Nature.

of 10^{-15} N m^2) brain-penetrating probes for neural recordings, in which polymer needle substrates (a width of 10 μm and a thickness of 1.5 μm) serve as supports for thin metal pads and interconnects (the inset, 500 nm thick Au layers).[28] Here, carbon fibers (7-μm-diameter) allow for mechanical insertion of these soft probes into brain tissues as chronic implants. Related systems involve open mesh constructs, as shown in Fig. 1(b), delivered via syringe injection into the depths of tissues to establish a distributed electronic interface.[29] Another platform relies on thin, flexible sheets [Fig. 1(c)], distinguished relative to the other two examples by the use of active electronics based on silicon-nanomembrane (Si-NM) transistors for active matrix addressing and local amplification in high resolution spatiotemporal mapping of electrophysiological activity from curved surfaces of the brain.[30]

PERSPECTIVES ON THIN, FLEXIBLE ENCAPSULATION MATERIALS

Encapsulation for these systems represents a key challenge and is the focus of recent research, where the goal is for chronic stability and, ultimately, safe and robust operation over time scales that can span the lifetime of the animal models or the patients, for biomedical research or human healthcare, respectively. Some examples of promising approaches appear in Fig. 2. Early techniques for the types of systems highlighted in Fig. 1(c) involve thin, spin cast layers of epoxy based polymers,[31] as in Fig. 2(a), where arrays of interconnected Si-NM transistors on a polyimide substrate (~25 μm, Kapton film) are protected in this way, with the epoxy (~20-μm thick layer, SU-8, MicroChem) photopatterned to leave the measurement electrodes exposed. Another strategy uses relatively thick coatings of silicone elastomer [poly(dimethylsiloxane), PDMS, 700 μm, formed by drop casting] bonded on top of thin, flexible Si-CMOS circuits based on Si-NM transistors on polyimide substrates in buckled configurations.[32] These "wavy" shapes, taken together with the low modulus, elastic mechanics of the PDMS, yield systems that can both bend and stretch with performance comparable to otherwise similar systems built on rigid, planar semiconductor wafers [Fig. 2(b)]. The compliant mechanics allows for intimate contacts to dynamic tissue surfaces.

The challenge with polymers such as polyimide, epoxy, and silicone is that their intrinsic barrier properties are limited by finite rates of water permeation, thereby limiting functional lifetimes as *in vivo* implants to time scales of days, weeks, or several months, typically. The water vapor transmission rate [WVTR, unit as (g/m^2)/day][33] serves as a useful comparative metric for the permeability across various barrier coatings and multilayers. Figure 2(c) illustrates the range of requirements for various different types of flexible electronic devices at specific conditions [i.e., 25 °C and 100% relative humidity (RH)], together with some data on different barriers based on recent reports.[33–35] Popular polymers (i.e., SU-8, Parylene C, polyimide, etc.) generally show high rates of permeation when used as films with micron-scale thicknesses, either spin coated (polyimide) or deposited from the vapor phase (Parylene C). Specific values range from 10^2 to 10° (g/m^2)/day.[33,34,36] Inorganic materials

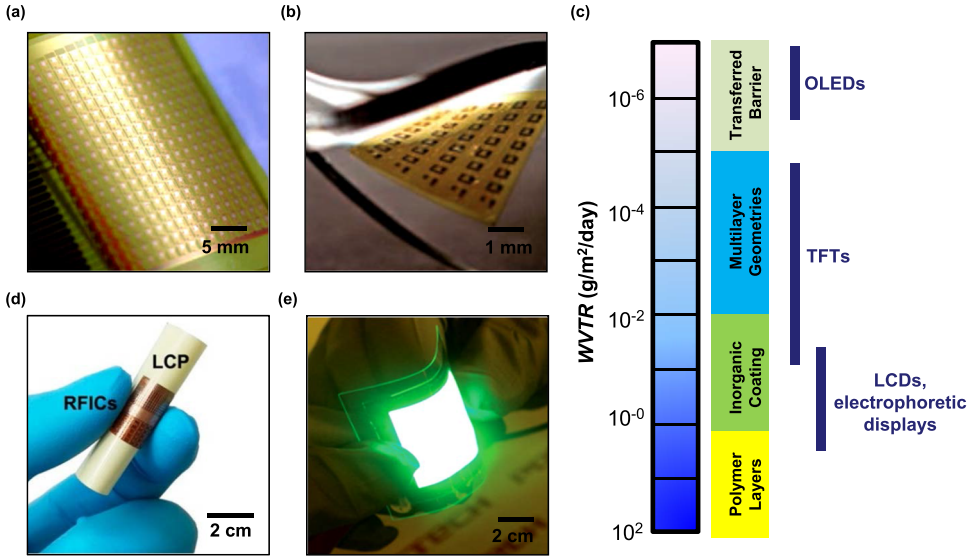

FIG. 2. Encapsulation materials in bio-electronics and in other functional systems. (a) Photograph of a thin, flexible system of electronics that supports actively multiplexed, amplified operation, encapsulated by a thin layer of photopatterned epoxy. Reproduced with permission from Viventi *et al.*, Sci. Transl. Med. **2**(24), 24ra22 (2010). Copyright 2010 AAAS. (b) Images of a twisted Si-CMOS circuit in a thin, "wavy" geometry (~1.4 mm thick), encapsulated in PDMS. Reproduced with permission from Viventi *et al.*, Sci. Transl. Med. **2**(24), 24ra22 (2010). Copyright 2008 AAAS. (c) Illustration of the range of rates of water permeation [WVTR, water vapor transmission rate, unit as (g/m^2)/day] for materials used to encapsulate common flexible electronic devices such as OFETs (organic field-effect transistors), TFTs (thin-film transistors), and LCDs (liquid crystal displays). Reproduced with permission from Choi *et al.*, Prog. Polym. Sci. **33**, 581 (2008). Copyright 2008 Elsevier. (d) Photograph of flexible RFICs (radio frequency integrated circuits) with 50-μm thick layers of LCP for encapsulation, showing that the LCP can provide conformal contact on curvilinear surfaces. Reproduced with permission from Hwang *et al.*, ACS Nano **7**(5), 4545 (2013). Copyright 2013 American Chemical Society. (e) Flexible OLED supported by a Fe–Ni alloy metal foil (40 μm thickness). Reproduced with permission from Park *et al.*, Adv. Mater. **27**, 4308 (2015). Copyright 2015 John Wiley and Sons.

(i.e., SiN_x Al_2O_3, etc.) grown directly by techniques such as atomic layer deposition (ALD) and chemical vapor deposition (CVD) offer superior properties.[37–39] Nevertheless, in most cases, particularly those encountered in research laboratories, extrinsic limitations associated with heterogeneities in the growth processes, surface relief on the target surface and other chemical effects, and/or contaminants almost invariably lead to some density of micro/nanoscale material defects (i.e., pinholes, cracks, nanopores, and grain boundaries) that are difficult or impossible to eliminate entirely over areas (~cm^2) of interest for many classes of implants. Approaches that further improve barrier performance [~10^{-4} (g/m^2)/day] adopt multilayer geometries [Fig. 2(c)], commonly as alternating stacks of organic/inorganic materials, to reduce the potential for such types of defects to extend throughout the thickness. For example, multibilayer structures of Al_2O_3/ZrO_2 (ALD, 2 nm/2 nm) with total thicknesses of 30 nm can effectively encapsulate films of calcium (Ca) (over 1 cm^2, 200 nm thickness) exposed at 85 °C to 85% RH for several days. Here, the electrical conductance of the underlying Ca film decreases as water vapor transmits through the barrier to oxidize Ca, consistent with a WVTR of 2×10^{-4} (g/m^2)/day.[40] In practical systems, additional challenges arise from difficulties in forming such coatings on prefabricated electronic systems that present complex topography and widely varying surface chemistries. Further constraints stem from requirements that the deposition and associated processing conditions (temperatures, chemistries, plasma parameters, etc.) must be compatible with the electronics.

Recent work demonstrates the utility of an alternative material strategy that circumvents these issues, wherein the fabrication sequence begins with the separate, unconstrained formation of the encapsulation layer on an ideal substrate surface such as that of a device-grade semiconductor wafer [Fig. 2(c)].[41] Next, a series of processing steps performed on the surface of this layer yield the necessary electronics such that removal of the substrate completes the fabrication. Alternatively, schemes for releasing the layer from its supporting substrate allow its physical transfer onto separately fabricated electronic systems. Both routes exploit fully optimized conditions for forming these layers, such as deposition/annealing temperatures, pressures, chemical/plasma exposures, and substrate surfaces/chemistries, selected without considerations associated with the materials and devices of the active/passive components of the electronics. Additional encapsulation of the backsides of the resulting platforms can occur via another cycle of physical transfer. This decoupling of device fabrication from encapsulation has many benefits, including applicability across a range of different material types.

Figure 2(d) illustrates the use of preformed layers of liquid-crystal-polymer (LCP, 50 μm) with separately fabricated Si-NM radio frequency integrated circuits (RFICs) in examples of retinal and subcutaneous implants.[42] Here, lamination of the LCP on the top and bottom sides of the electronics provides robust barrier function *in vivo* and projected lifetimes of ~2 years when immersed in phosphate-buffered solution (PBS) at 37 °C. Similarly, Fig. 2(e) demonstrates the ability of a thin Fe–Ni alloy foil (40 μm) to serve as a substrate and bottom side encapsulation for an array of OLEDs (organic light-emitting diodes). By monitoring the conductance of an underlying Ca film encapsulated by this foil at constant voltage and at 25 °C, 40% RH, suggests a WVTR of 5.5×10^{-4} (g/m^2)/day.[43] These options are interesting, but they are highly nonideal for bio-integrated electronic systems. Both require thicknesses in the range of tens of microns, thereby limiting the degree of mechanical flexibility and preventing capacitive interfaces for electrical measurement and/or stimulation. Additionally, metal foils do not allow for electromagnetic coupling between the devices and the surrounding biology.

PHYSICALLY TRANSFERRED LAYERS OF THERMALLY GROWN SiO_2 AS ENCAPSULATION MATERIALS

Recent efforts to bypass these disadvantages focus on the use of submicron thick layers of SiO_2 created by thermal growth on the surfaces of device-grade silicon wafers.[23] Formation of SiO_2 in this manner (which we refer to here as t-SiO_2) yields layers of material that are uniform, dense, and free of defects due to the pristine chemistry and flat topography of the supporting substrate and the optimized conditions (thermal oxidation, ~1100 °C) of the growth processes.[44] The resulting films are far superior to SiO_2 thin films formed in other ways, including those based on sol-gel processing, CVD, or ALD.[45] A combination of dry and wet etching, and/or mechanical grinding, removes the silicon wafer to expose the bottom surface of t-SiO_2 as a biocompatible measurement interface or to release the film for subsequent physical transfer onto a preformed device platform.[41,44] Figure 3(a) shows an array of patterns of magnesium (Mg) ("I"-shape logo for the University of Illinois) (left) and an active matrix system for electrophysiological mapping (a collection of 252 Si-NM transistors, 18 rows by 14 columns) (right) encapsulated by transferred layers of t-SiO_2 with thicknesses of 100 nm and 900 nm, respectively.[41] This barrier structure can be integrated across the surfaces of flexible electronic devices with areas limited only by the dimensions of the growth wafer. The thin geometries support excellent levels of bendability and, in their bonded configuration, sufficient mechanical robustness [Fig. 3(b)]. The transparency of t-SiO_2 allows for optical access,[46] and the electrically insulating properties and the small thicknesses can support capacitive measurement and/or stimulation interfaces.[47]

Accelerated tests of t-SiO_2-encapsulated electronics involve complete immersion in solutions of PBS (pH 7.4, 70 °C). Representative results are in Fig. 3(c) with molecular dynamics simulations[41] that reveal the critical chemical aspects of t-SiO_2 dissolution in phosphate-buffered solution (PBS) [$SiO_2 + 2H_2O \rightarrow Si(OH)_4$].[48] The simplest reaction involves the fast formation of a Si–OH bond between a water molecule (w1) and a Si atom. The reaction with a second water molecule (w2) then follows, leading to a final product of silicic acid [$Si(OH)_4$] in the solution. Temperature-dependent measurements of the rates of hydrolysis of t-SiO_2 in PBS are in Fig. 3(d). The results are consistent with Arrhenius scaling and an activation energy of E_A = 1.32 eV.[41] A collection of SEM images (right) highlight the controlled, systematic, spatially uniform nature of the reductions in the thickness of t-SiO_2 as a function of time of immersion in PBS at 96 °C. The results suggest that the limiting consideration for use of t-SiO_2 as a biofluid barrier is in this slow hydrolysis process (~15 nm/year at 37 °C), as opposed to effects associated with defects or water permeation.[41] In addition to water, certain species of ions such as sodium (Na^+) in biofluids can also potentially diffuse through barriers, thereby degrading certain properties of the underlying electronics. To address this issue, capping layers of SiN_x[49] by CVD or HfO_2 by ALD[50] can be included to block

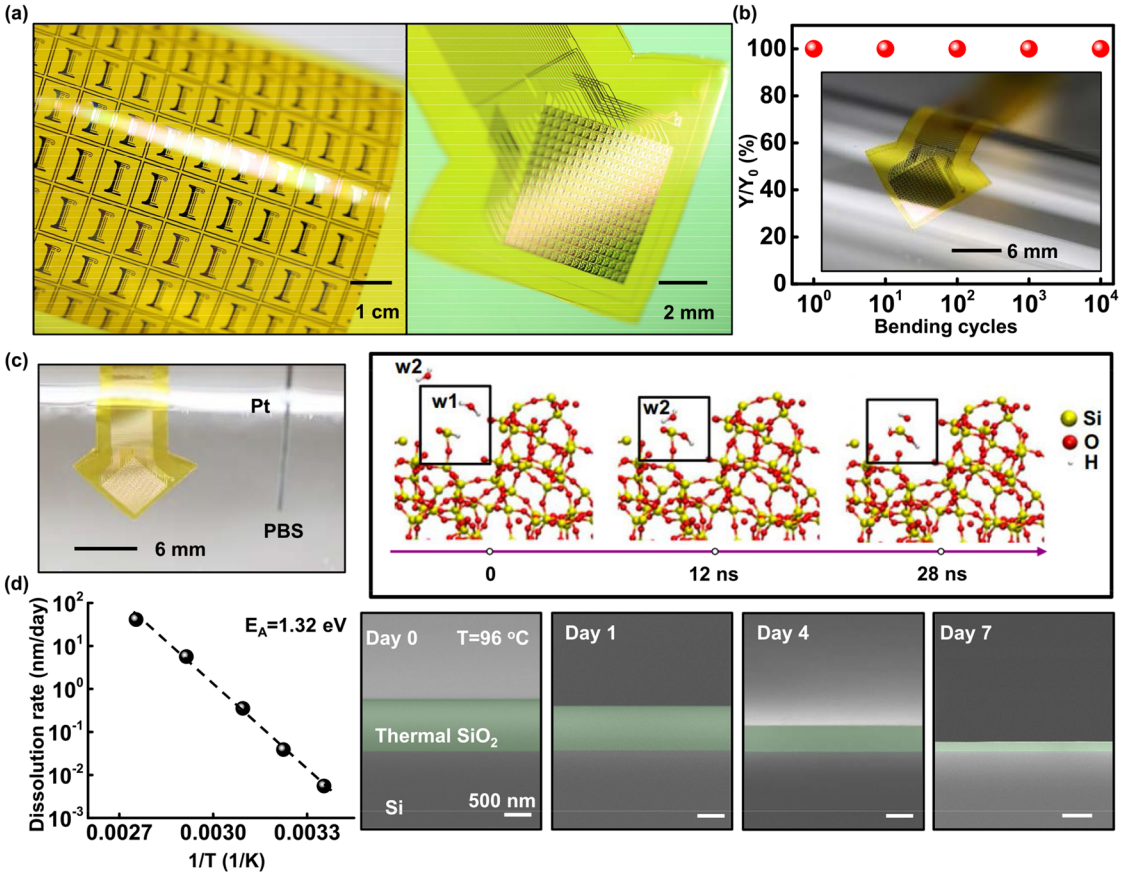

FIG. 3. Thermally grown layers of SiO_2 as encapsulation materials for flexible electronic systems. (a) Optical image of an array of patterns of Mg (left) and an active matrix circuit (right) encapsulated by a layer of t-SiO_2 with thicknesses of 100 nm and 900 nm, respectively. (b) Demonstration of bendability of the circuit system. Y/Y_0 is defined as the ratio of the number of working transistors and the total number of transistors. (c) Results of immersion tests [PBS (phosphate-buffered solution) at 70 °C, a pH of 7.4] and simulations of the associated chemical reactions. (d) Dissolution rate of t-SiO_2 at different temperatures (left). Series of images of the process of dissolution of a layer of SiO_2 (1 μm) soaked in PBS within 7 days at 96 °C (right). Reproduced with permission from Fang *et al.*, Proc. Natl. Acad. Sci. U. S. A. **113**(42), 11682 (2016). Copyright 2016 National Academy of Sciences.

ion transport[51] and/or to retard the hydrolysis of t-SiO_2,[50,52] thereby offering a prolonged longevity of systems and stability of operation.

Comparisons to various encapsulation materials formed by other techniques (e.g., spin-casting, ALD, and CVD) follow from soak tests using setups that incorporate Mg films, as in Table I. Here, the reaction of Mg with water that penetrates through the encapsulation layers yields $Mg(OH)_2$ and, by consequence, a readily visible change in optical properties that can be monitored by optical microscopy and/or visual inspection. The lifetimes of most layers can be defined as the first observable "pinhole" defect evaluated in this manner. As shown in Table I, a 100 nm thick layer of t-SiO_2 survives for over 22 days of complete immersion in 70 °C PBS at a pH of 7.4 (left in the first row), corresponding to a 30-h lifetime in 96 °C PBS, consistent with the hydrolysis rate in Fig. 3(d), without appearance of any localized defects throughout the testing process. Other inorganic/organic single/multilayer systems, each deposited in academic cleanroom facilities with commercial equipment to different thicknesses, exhibit rapid failure due to water permeation either through the materials themselves (e.g., spin-coated polymers) or through localized defects (e.g., inorganic materials) that commonly occur with densities between 1 and 5 per cm^2.[41] The defect-free structure, thin-film geometry, and ultralow permeability [~2×10^{-8} (g/m^2)/day for a case of 100 nm t-SiO_2 at 37 °C, 100% RH][53–55] of t-SiO_2 represent improvements over any other material system examined, as summarized in Fig. 2.

THERMALLY GROWN SiO_2 AS ENCAPSULATING LAYERS IN ACTIVELY MULTIPLEXED, CAPACITIVELY COUPLED SYSTEMS FOR ELECTROPHYSIOLOGICAL MAPPING

Initial examples of t-SiO_2 for encapsulation of flexible, bio-integrated electronic systems focused on high-density, capacitively coupled devices with active multiplexed addressing and local buffering provided by a two dimensional array of Si NM transistors (Fig. 4), configured for electrophysiology mapping on dynamic,

TABLE I. Summary of comparative Mg soak test results for different barrier materials. Reproduced with permission from Fang *et al.*, Proc. Natl. Acad. Sci. U. S. A. **113**(42), 11682 (2016). Copyright 2016 National Academy of Sciences.

t-SiO_2 100 nm 70 °C, 22 day	PI2545 1 μm 37 °C, 20.5 h	Parylene C 1 μm 37 °C, 1.5 h	PDMS 1 μm 37 °C, 65 min	LCP 25 μm 70 °C, 9 day
				
PECVD low-dep SiO_2 1 μm 37 °C, 15 min	PECVD SiN_x 1 μm 37 °C, 25 min	ALD Al_2O_3 100 nm 37 °C, 10 min	ALD HfO_2 100 nm 37 °C, 80 min	SiO_2/SiN_x × 3 16.6/16.6 nm × 3 37 °C, 15 min
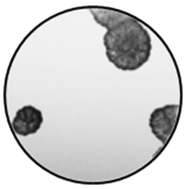		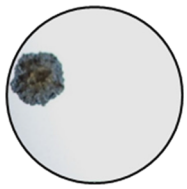		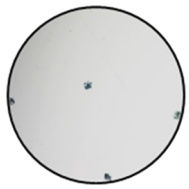
Al_2O_3/HfO_2 × 3 16.6/16.6 nm × 3 37 °C, 37 min	Al_2O_3/Parylene C 50/1000 nm 70 °C, 7.5 h	Al_2O_3/Parylene C 50/6000 nm 70 °C, 12 h	Al_2O_3/Parylene C × 3 50/283.3 nm × 3 37 °C, 50 min	Al_2O_3/PI2545 50/950 nm 37 °C, 30 min
	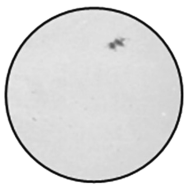			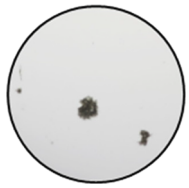
$Al_2O_3/PI2545$ × 3 50/283.3 nm × 3 37 °C, 13.5 h	HfO_2/Parylene C 50/950 nm 70 °C, 250 h	HfO_2/Parylene C × 3 50/283.3 nm × 3 70 °C, 46 min	HfO_2/PI2545 50/950 nm 37 °C, 5 h	HfO_2/PI2545 × 3 50/283.3 nm × 3 37 °C, 10 h
		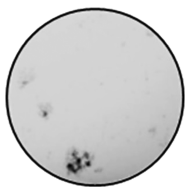		
SiN_x/Al_2O_3/Parylene C 50/50/900 nm 37 °C, 62.5 h	Ti/Pt 5/100 nm 37 °C, 5 min	Cr/Au 5/100 nm 37 °C, 5 min	Cr/Au 5/1000 nm 37 °C, 75 min	
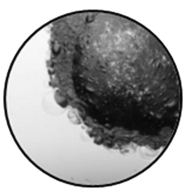	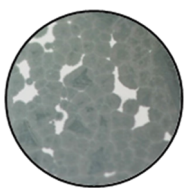	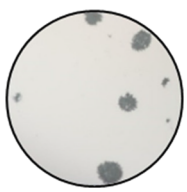	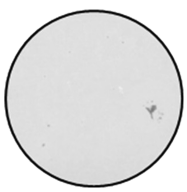	5 mm

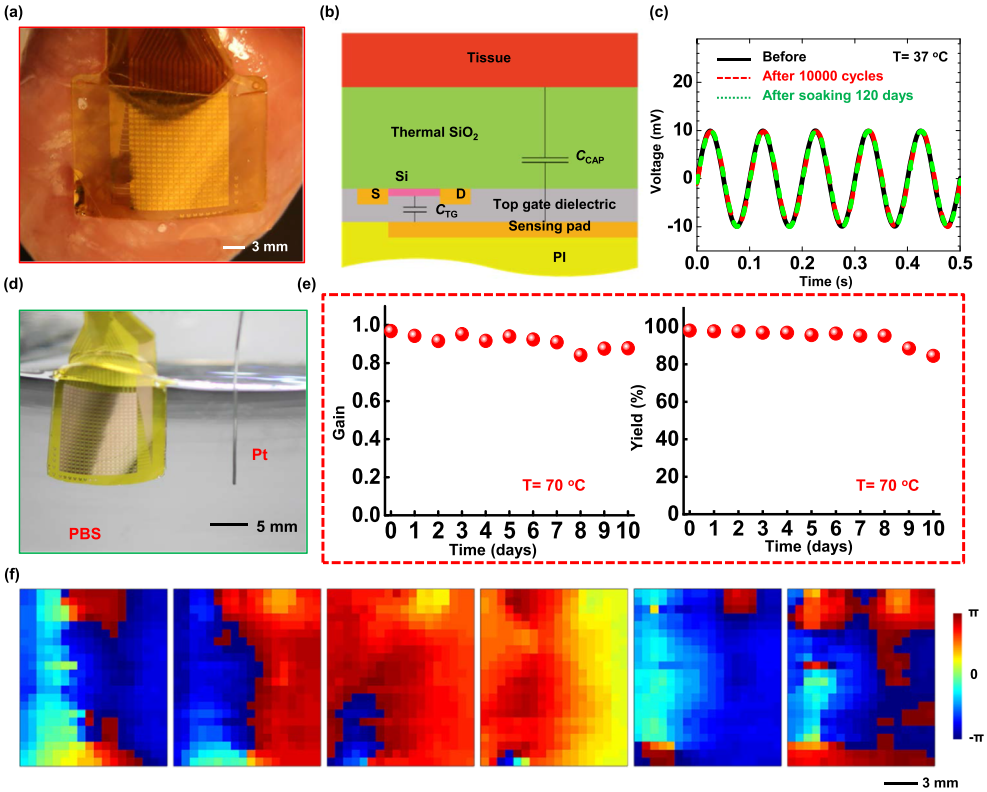

FIG. 4. Layers of t-SiO_2 for chronically stable encapsulation of capacitively coupled, actively multiplexed systems for electrophysiological mapping. (a) Optical image of conformal contact of a device on the cardiac tissue via the action of surface tension. (b) Schematic illustration of the circuit cross section to illustrate the mechanism for capacitively coupled sensing through a thermal SiO_2 layer to an underlying transistor. (c) The response of a representative channel in this system to a sine-wave input (at 10 Hz) before and after 10 000 cycles of bending and saline immersion (PBS, phosphate-buffered solution, at 37 °C) for 120 days. (d) Image of a device completely immersed in PBS, during a soak test. (e) Accelerated immersion tests (PBS at 70 °C) with *in vitro* measurement of active transistor electrode gain and yield. Reproduced with permission from Fang *et al.*, Proc. Natl. Acad. Sci. U. S. A. **113**(42), 11682 (2016). Copyright 2016 National Academy of Sciences. (f) Phase maps measured at different time points (over a period of 50 ms) during ventricular fibrillation. Reproduced with permission from Fang *et al.*, Nat. Biomed. Eng. **1**(3), 0038 (2017). Copyright 2017 Springer Nature.

curved surfaces of cardiac tissues.[47] Figure 4(a) highlights conformal contact between such a t-SiO_2-encapsulated system and a rabbit heart. Here, a uniform layer of t-SiO_2 [0.95 × 1.15 cm^2 with a thickness of 900 nm in Fig. 4(a)] serves as a barrier layer for an underlying sheet of flexible electronics that supports 396 multiplexed, capacitive measurement channels in a layout with 18 columns by 22 rows.[56] The principle of capacitive coupling to an electrode that interfaces with a Si-NM transistor at an individual channel appears in Fig. 4(b), where the biopotential associated with the tissue in contact with t-SiO_2 leads to a direct coupling to the semiconducting channel of a Si-NM transistor. Consequently, the presence of the high-impedance t-SiO_2 layer (~2.6 GΩ at 10 Hz) not only protects the electronics from biofluids but also enables biopotential recordings at tissue/SiO_2 interfaces. The former role favors larger thicknesses, while the latter favors smaller; a balance between these considerations yields systems that offer not only long-lived, reliable operation but also high fidelity recording capabilities for both cardiac and neural electrophysiology.

A summary of a series of soak and bending experiments on such platforms appears in Figs. 4(c) and 4(d).[56] The amplifier output response [Fig. 4(c)] to a 10-Hz sine-wave input before and after the soak (37 °C PBS with a pH of 7.4 for 120 days) and bending tests (5 mm radius for 1000 cycles) demonstrates that the electrical performance remains constant under these conditions. An image of a setup for related studies is in Fig. 4(d) for the case of full immersion in PBS. Similar evaluations, summarized in Fig. 4(e), involve temperature-accelerated aging tests (70 °C PBS for 10 days) of a system of actively multiplexed electronics with 252 sensing sites (14 columns by 18 rows), where a 900 nm thick layer of t-SiO_2 encapsulates both the top and bottom surfaces of the system.[41] The fabrication in this case involves laminating a separately prepared film of polyimide with a transferred thin t-SiO_2 layer on its top surface onto a preprocessed layer of electronics on an SOI (silicon-on-insulator) electronic platform followed by removing the bottom wafer to yield a flexible system protected on both systems by t-SiO_2. Uniform gain and yield values measured from such systems (gain corresponds to ratio between output and input voltages; yield is the number of working transistors divided by total transistor number) remain at high levels (gain ~1 and yield ~100%) after 10 days of immersion in 70 °C PBS, suggesting a lifetime of at least several decades at 37 °C by Arrhenius scaling.

Figure 4(f) illustrates the application of a device of this type for high resolution spatiotemporal mapping of electrical activity associated with ventricular fibrillation, characterized by disorganized cardiac electrical activity.[56] Here, the capacitively coupled array records biopotentials [i.e., electrocardiogram (ECG) recordings] with layers of t-SiO_2 as encapsulation and sensing interfaces across the surface of an isolated rabbit heart [as shown in Fig. 4(a)]. The results yield electrophysiological phase maps recorded at 6 sequential time points (over a period of 50 ms) from the heart during ventricular fibrillation. As a clinical method for assessing arrhythmias, calculation of single phase values can identify the location of phase singularities via analysis of these maps [Fig. 4(f)]. These representative demonstrations suggest broad applicability of t-SiO_2-encapsulated, flexible bio-integrated electronic systems as stable, biocompatible interfaces for long-lived recordings.[48,57]

THERMALLY GROWN LAYERS OF SiO_2 AND HIGHLY DOPED LAYERS OF MONOCRYSTALLINE SILICON IN ACTIVELY MULTIPLEXED, CONDUCTIVELY COUPLED SYSTEMS FOR ELECTROPHYSIOLOGICAL MAPPING AND STIMULATION

Despite these advantages of t-SiO_2, one fundamental limitation is in the requirement for capacitive coupling in electrical sensing and/or stimulation. Consequently, although useful in many scenarios of interest, system layouts favor large sensing pads and thin

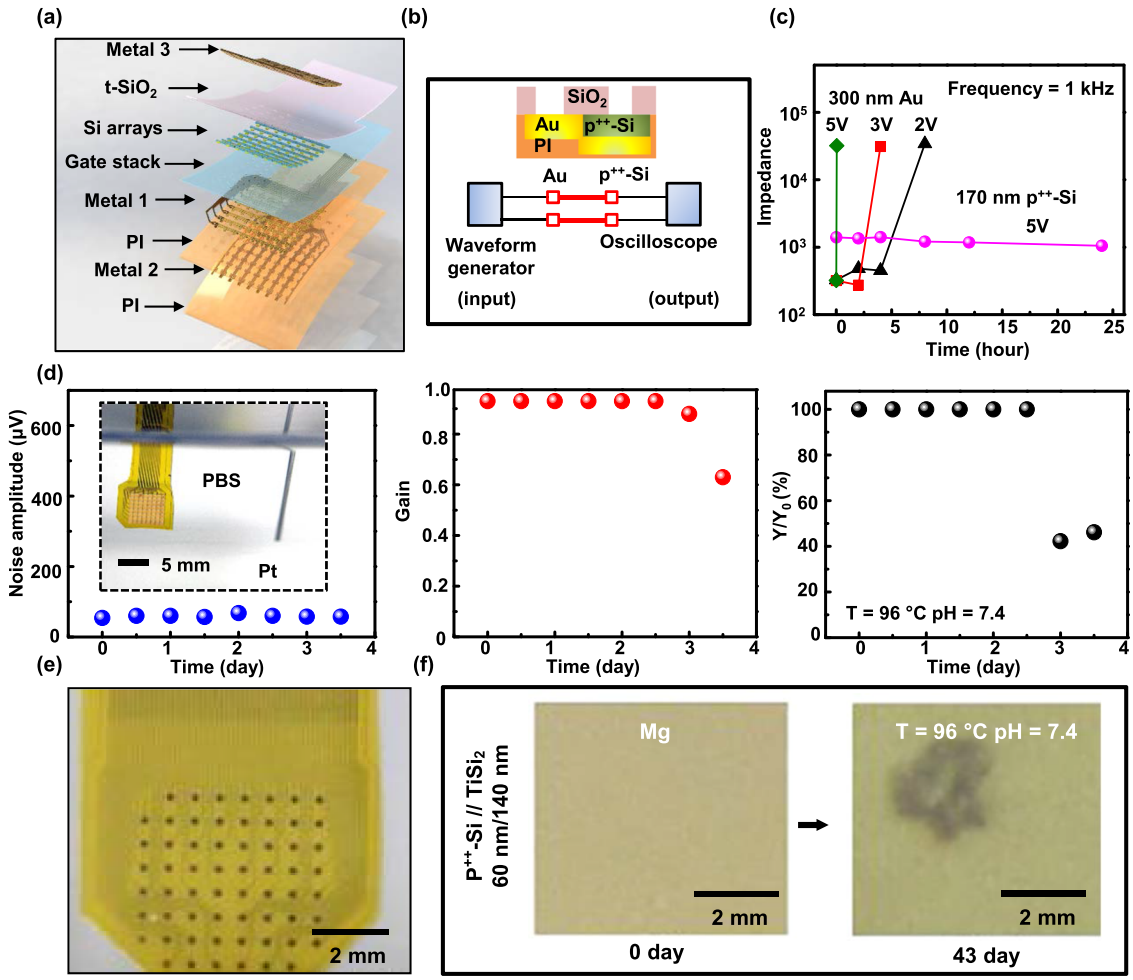

FIG. 5. Constructs of t-SiO_2 and doped Si for chronically stable encapsulation of conductively coupled, actively multiplexed systems for electrophysiological mapping and stimulation. (a) Design and characterization of an actively multiplexed array of conductively coupled sensors for electrophysiological mapping, with the p^{++}–Si//t-SiO_2 structure as an interface. (b) Circuit diagram of the impedance test system with annotations for each component. (c) Comparison results that illustrate the lifetimes of a p^{++}–Si electrode (3×3 mm^2, 170 nm thickness) and a Au electrode (3×3 mm^2, 300 nm thickness) operated at different simulation voltages. (d) Accelerated immersion tests (PBS at 96 °C) with *in vitro* measurement of transistor electrode noise amplitude, gain, and yield. The performance remains stable until failure at day 3. Reproduced with permission from Li *et al.*, Proc. Natl. Acad. Sci. U. S. A. **115**(41), E9542 (2018). Copyright 2018 National Academy of Sciences. (e) Photograph of a 61 channel passive electrode system encapsulated by $TiSi_2$ materials in the flexible form. (f) Optical images of Mg in a representative test device immersed in PBS (pH = 7.4) at 96 °C. Reproduced with permission from Li *et al.*, ACS Nano **13**, 660 (2019). Copyright 2019 American Chemical Society.

geometries in t-SiO_2. As a result, simultaneous scaling of designs to allow both fine resolution and extreme longevity can be difficult. A recent study presents a solution to this challenge that exploits an interface that consists of highly doped Si (p^{++}–Si, ~10^{20} cm^{-3} boron dopants) NMs intimately bonded to a layer of t-SiO_2 in a sealed, monolithic structure. In this context, the p^{++}–Si-NM serves as the basis of a Faradaic interface between the electronics and the targeted biological tissues through a small opening through t-SiO_2.[58] This construct allows for direct interactions of charges in the surrounding solution with a conductive path to the Si NM transistors in the associated electronics, of relevance to both electrical recording and stimulation [Fig. 5(a)].[59]

Figure 5(b) presents a circuit diagram of a flexible system of stimulation electrodes encapsulated with this type of structure, which we designate as p^{++}–Si//t-SiO_2. Impedance measurements of electrochemical stability, as shown in Fig. 5(c), follow published procedures for pulsed-mode stimulation of neural and cardiac systems.[59] An otherwise similar system based on Au as an interface electrode exhibits evidence of reaction of Au with ions in the solution within a short period of time in the presence of a voltage due to the formation of soluble complexes. By contrast, the electrode encapsulated with 170 nm thick p^{++}–Si exhibits stable impedance values with an extended lifetime limited by the dissolution of Si (after 3-day soaking in 96 °C PBS, a pH of 7.4) even at high voltages (5 V input). The results indicate that this material construct can act as both an electrical interface and encapsulation layer for stimulation electrodes.

Sensing electrodes of p^{++}–Si (60 nm)//t-SiO_2 (1 μm) can be interfaced monolithically with Si-NM transistors for electrophysiological mapping with an active matrix readout, analogous to the capacitively coupled systems described previously. This design contains an amplifier for conductive sensing via p^{++}–Si//t-SiO_2 to the gate electrode. The Faradaic contact largely circumvents limitations in resolution associated with the size of the sensing pad and in coupling strength due to the thickness of t-SiO_2. The fill factor (defined by the ratio of the cumulative area of the electrodes to the total area of the system) can approach values close to 100% even though the p^{++}–Si regions have a fill factor of only ~5% or less. Figure 5(d) shows stable electrical performance during full immersion in PBS at 96 °C for three days, corresponding to the complete dissolution of the 170 nm thick layer of p^{++}–Si. The absence of significant changes of noise amplitude, gain, and yield within this lifetime (<3 days) highlights the stability of such system, results of which can be projected to a lifetime over 1 year at 37 °C.[59]

These results reveal that the limiting factor in these systems is the relatively high dissolution rate of p^{++}–Si compared to that of t-SiO_2 (p^{++}–Si: ~5 nm/day in 37 °C PBS, pH 7.4 for a case of 10^{20} cm^{-3} boron dopants).[58] A recent study indicates that replacing silicon with a bilayer structure of a metal silicide alloy (i.e., p^{++}–Si/$TiSi_2$) and silicon enhances operating lifetimes of these types of implantable electronics by orders of magnitude.[60] In this case, $TiSi_2$, formed by the high-temperature reaction of thin metal films (titanium, Ti) deposited on monocrystalline silicon, represents an attractive choice due to its biocompatibility, its high conductivity, and its relatively low cost. Figure 5(e) displays an optical image of a 61-channel passive system in the flexible form, with encapsulation layers of p^{++}–Si/$TiSi_2$.[60] Soak tests with Mg films using setups described previously show excellent chronic stability (within 43 days) of such barrier (p^{++}–Si/$TiSi_2$, 60/140 nm) during immersion in 96 °C PBS (a pH of 7.4) [Fig. 5(f)]; indicating the projected water-permeation rate of $TiSi_2$ at 37 °C (~0.14 nm per year)[60] is lower by orders of magnitude than that of t-SiO_2 (~15 nm per year).[41] Consequently, such systems offer great potential for long-term, high-performance bioelectronics.

CHALLENGES AND FUTURE DIRECTIONS

As highlighted in this article, advances in materials and integration strategies are essential to the successful development of chronically stable, flexible bio-electronic implants. The performance of Si-based thin films (i.e., Si, SiO_2, and $TiSi_2$) derived from wafer-based sources of material appears to solve most of the key challenges; extensions and/or adaptations of the basic concepts will likely lead to further progress and opportunities. An additional area for future work is to build on these approaches or to develop alternatives that can support not only bending but also stretching and twisting deformations that require low-modulus, large-strain deformations, as demanded by integration with certain complex biological surfaces. In all cases, biocompatibility at the level of the materials themselves is important to consider as immunogenic scar formation and other tissue reactions can isolate electrodes from target cells and tissues, thereby reducing the effective lifetime of the entire system even if the barrier properties are not compromised. Here, coatings of conductive, functionalized polymers or synthetic/biological hybrids or drug-eluting materials may have important roles. At the system level, opportunities exist in the development of platforms for closed-loop, real-time feedback and adaptive response in advanced neuroengineering and neuromodulation. Insights gained from the use of such technologies and those summarized previously through *in vivo* studies and trials in freely moving animal models will accelerate further progress. These types of interdisciplinary efforts represent fertile areas for research programs spanning biomedical research to human healthcare.

ACKNOWLEDGMENTS

We acknowledged support from the Center for Bio-Integrated Electronics at Northwestern University.

REFERENCES

[1] J. J. Jun, N. A. Steinmetz, J. H. Siegle, D. J. Denman, M. Bauza, B. Barbarits, A. K. Lee, C. A. Anastassiou, A. Andrei, Ç. Aydın, M. Barbic, T. J. Blanche, V. Bonin, J. Couto, B. Dutta, S. L. Gratiy, D. A. Gutnisky, M. Häusser, B. Karsh, P. Ledochowitsch, C. M. Lopez, C. Mitelut, S. Musa, M. Okun, M. Pachitariu, J. Putzeys, P. D. Rich, C. Rossant, W. Sun, K. Svoboda, M. Carandini, K. D. Harris, C. Koch, J. O'Keefe, and T. D. Harris, Nature **551**, 232 (2017).
[2] T. M. Fu, G. Hong, R. D. Viveros, T. Zhou, and C. M. Lieber, Proc. Natl. Acad. Sci. U. S. A. **114**, E10046 (2017).
[3] J. T. Robinson, M. Jorgolli, A. K. Shalek, M.-H. Yoon, R. S. Gertner, and H. Park, Nat. Nanotechnol. **7**, 180 (2012).
[4] D. Khodagholy, J. N. Gelinas, T. Thesen, W. Doyle, O. Devinsky, G. G. Malliaras, and G. Buzsaki, Nat. Neurosci. **18**, 310 (2015).
[5] B. Z. Tian, T. Cohen-Karni, Q. Qing, X. J. Duan, P. Xie, and C. M. Lieber, Science **329**, 830 (2010).
[6] F. Ershad, K. Sim, A. Thukral, Y. S. Zhang, and C. Yu, APL Mater. **7**, 031301 (2019).

[7]L. Xu, S. R. Gutbrod, A. P. Bonifas, Y. Su, M. S. Sulkin, N. Lu, H.-J. Chung, K.-I. Jang, Z. Liu, M. Ying, C. Lu, R. C. Webb, J.-S. Kim, J. I. Laughner, H. Cheng, Y. Liu, A. Ameen, J.-W. Jeong, G.-T. Kim, Y. Huang, I. R. Efimov, and J. A. Rogers, Nat. Commun. **5**, 3329 (2014).
[8]K. L. Montgomery, A. J. Yeh, J. S. Ho, V. Tsao, S. M. Iyer, L. Grosenick, E. A. Ferenczi, Y. Tanabe, K. Deisseroth, S. L. Delp, and A. S. Y. Poon, Nat. Methods **12**(10), 969 (2015).
[9]T. Kim, J. G. McCall, Y. H. Jung, X. Huang, E. R. Siuda, Y. Li, J. Song, Y. M. Song, H. A. Pao, R.-H. Kim, C. Lu, S. D. Lee, I.-S. Song, G. Shin, R. Al-Hasani, S. Kim, M. P. Tan, Y. Huang, F. G. Omenetto, J. A. Rogers, and M. R. Bruchas, Science **340**(6129), 211 (2013).
[10]A. Canales, X. Jia, U. P. Froriep, R. A. Koppes, C. M. Tringides, J. Selvidge, C. Lu, C. Hou, L. Wei, Y. Fink, and P. Anikeeva, Nat. Biotechnol. **33**(3), 277 (2015).
[11]D. Son, J. Lee, S. Qiao, R. Ghaffari, J. Kim, J. E. Lee, C. Song, S. J. Kim, D. J. Lee, S. W. Jun, S. Yang, M. Park, J. Shin, K. Do, M. Lee, K. Kang, C. S. Hwang, N. Lu, T. Hyeon, and D.-H. Kim, Nat. Nanotechnol. **9**(5), 397 (2014).
[12]D. J. Lipomi, M. Vosgueritchian, B. C. Tee, S. L. Hellstrom, J. A. Lee, C. H. Fox, and Z. Bao, Nat. Nanotechnol. **6**(12), 788 (2011).
[13]M. C. McAlpine, H. Ahmad, D. Wang, and J. R. Heath, Nat. Mater. **6**(5), 379–384 (2007).
[14]W. Gao, S. Emaminejad, H. Y. Nyein, S. Challa, K. Chen, A. Peck, H. M. Fahad, H. Ota, H. Shiraki, D. Kiriya, D. H. Lien, G. A. Brooks, R. W. Davis, and A. Javey, Nature **529**(7587), 509 (2016).
[15]W. Wu, L. Wang, Y. Li, F. Zhang, L. Lin, S. Niu, D. Chenet, X. Zhang, Y. Hao, T. F. Heinz, J. Hone, and Z. L. Wang, Nature **514**(7523), 470 (2014).
[16]M. Kaltenbrunner, T. Sekitani, J. Reeder, T. Yokota, K. Kuribara, T. Tokuhara, M. Drack, R. Schwödiauer, I. Graz, S. Bauer-Gogonea, S. Bauer, and T. Someya, Nature **499**(7459), 458 (2013).
[17]E. Song, R. Li, X. Jin, H. Du, Y. Huang, J. Zhang, Y. Xia, H. Fang, Y. K. Lee, K. J. Yu, J.-K. Chang, Y. Mei, M. A. Alam, Y. Huang, and J. A. Rogers, ACS Nano **12**, 10317 (2018).
[18]N. Thejo Kalyani and S. J. Dhoble, Renewable Sustainable Energy Rev. **44**, 319 (2015).
[19]X. Xie, L. Ritch, S. Mcrugu, P. Tathircddy, and F. Solzbacher, Appl. Phys. Lett. **101**(9), 093702 (2012).
[20]L. Bowman and J. D. Meindl, IEEE Trans. Biomed. Eng. **BME-33**(2), 248 (1986).
[21]J.-S. Park, H. Chae, H. K. Chung, and S. I. Lee, Semicond. Sci. Technol. **26**(3), 034001 (2011).
[22]H. S. Mayberg, A. M. Lozano, V. Voon, H. E. McNeely, D. Seminowicz, C. Hamani, J. M. Schwalb, and S. H. Kennedy, Neuron **45**(5), 651 (2005).
[23]C. S. Mestais, G. Charvet, F. Sauter-Starace, M. Foerster, D. Ratel, and A. L. Benabid, IEEE T. Neural Syst. Rehabil. Eng. **23**(1), 10 (2015).
[24]Y.-F. Zhang, S.-L. Bai, M. Miao, and Y.-F. Jin, J. Eur. Ceram. Soc. **29**, 1077–1082 (2009).
[25]K. A. Peterson, K. D. Patel, C. K. Ho, S. B. Rohde, C. D. Nordquist, C. A. Walker, B. D. Wroblewski, and M. Okandan, Int. J. Appl. Ceram. Technol. **2**(5), 345 (2005).
[26]P. J. Rousche and R. A. Normann, IEEE Trans. Rehabil. Eng. **7**, 56 (1999).
[27]B. S. Wilson, C. C. Finley, D. T. Lawson, R. D. Wolford, D. K. Eddington, and W. M. Rabinowitz, Nature **352**(6332), 236 (1991).
[28]L. Luan, X. Wei, Z. Zhao, J. J. Siegel, O. Potnis, C. A. Tuppen, S. Lin, S. Kazmi, R. A. Fowler, and S. Holloway, Sci. Adv. **3**, e1601966 (2017).
[29]J. Liu, T.-M. Fu, Z. Cheng, G. Hong, T. Zhou, L. Jin, M. Duvvuri, Z. Jiang, P. Kruskal, C. Xie, Z. Suo, Y. Fang, and C. M. Lieber, Nat. Nanotechnol. **10**, 629 (2015).
[30]J. Viventi, D.-H. Kim, L. Vigeland, E. S. Frechette, J. A. Blanco, Y. S. Kim, A. E. Avrin, V. R. Tiruvadi, S.-W. Hwang, A. C. Vanleer, D. F. Wulsin, K. Davis, C. E. Gelber, L. Palmer, J. Van der Spiegel, J. Wu, J. Xiao, Y. Huang, D. Contreras, J. A. Rogers, and B. Litt, Nat. Neurosci. **14**, 1599 (2011).
[31]J. Viventi, D.-H. Kim, J. D. Moss, Y.-S. Kim, J. A. Blanco, N. Annetta, A. Hicks, J. L. Xiao, Y. Huang, D. J. Callans, J. A. Rogers, and B. Litt, Sci. Transl. Med. **2**(24), 24ra22 (2010).
[32]D.-H. Kim, J.-H. Ahn, W. M. Choi, H.-S. Kim, T.-H. Kim, J. Song, Y. Huang, Z. Liu, C. Lu, and J. A. Rogers, Science **320**, 507 (2008).
[33]J. Ahmad, K. Bazaka, L. J. Anderson, R. D. White, and M. V. Jacob, Renewable Sustainable Energy Rev. **27**, 104 (2013).
[34]M.-C. Choi, Y. Kim, and C.-S. Ha, Prog. Polym. Sci. **33**, 581 (2008).
[35]J. Lewis, Mater. Today **9**(4), 38 (2006).
[36]T.-N. Chen, D.-S. Wuu, C.-C. Wu, C.-C. Chiang, Y.-P. Chen, and R.-H. Horng, Plasma Processes Polym. **4**, 180 (2007).
[37]J. Jeong, F. Laiwalla, J. Lee, R. Ritasalo, M. Pudas, L. Larson, V. Leung, and A. Nurmikko, Adv. Funct. Mater. **29**, 1806440 (2019).
[38]D. Yu, Y.-Q. Yang, Z. Chen, Y. Tao, and Y.-F. Liu, Opt. Commun. **362**, 43 (2016).
[39]M. D. Groner, S. M. George, R. S. McLean, and P. F. Carcia, Appl. Phys. Lett. **88**, 051907 (2006).
[40]S.-W. Seo, E. Jung, H. Chae, and S. M. Cho, Org. Electron. **13**, 2436 (2012).
[41]H. Fang, J. Zhao, K. J. Yu, E. Song, A. B. Farimani, C.-H. Chiange, X. Jin, Y. Xue, D. Xu, W. Dui, K. J. Seo, Y. Zhong, Z. Yang, S. M. Won, G. Fang, S. W. Choi, S. Chaudhuri, Y. Huang, M. A. Alam, J. Viventi, N. R. Aluru, and J. A. Rogers, Proc. Natl. Acad. Sci. U. S. A. **113**(42), 11682 (2016).
[42]G.-T. Hwang, D. Im, S. E. Lee, J. Lee, M. Koo, S. Y. Park, S. Kim, K. Yang, S. J. Kim, K. Lee, and K. J. Lee, ACS Nano **7**(5), 4545 (2013).
[43]M.-H. Park, J.-Y. Kim, T.-H. Han, T.-S. Kim, H. Kim, and T.-W. Lee, Adv. Mater. **27**, 4308 (2015).
[44]G. Li, E. Song, G. Huang, R. Pan, Q. Guo, F. Ma, Z. Di, B. Zhou, and Y. Mei, Adv. Funct. Mater. **28**, 1801448 (2018).
[45]S.-K. Kang, S.-W. Hwang, H. Cheng, S. Yu, B. H. Kim, J.-H. Kim, Y. Huang, and J. A. Rogers, Adv. Funct. Mater. **24**, 4427 (2014).
[46]G. Li, E. Song, G. Huang, R. Pan, Q. Guo, F. Ma, Z. Di, B. Zhou, and Y. Mei, Small **14**, 1802985 (2018).
[47]M. Y. Rotenberg and B. Tian, Nat. Biomed. Eng. **1**, 0048 (2017).
[48]Y. K. Lee, K. J. Yu, Y. Kim, Y. Yoon, Z. Xie, E. Song, H. Luan, X. Feng, Y. Huang, and J. A. Rogers, ACS Appl. Mater. Interfaces **9**(49), 42633 (2017).
[49]E. Song, H. Fang, X. Jin, J. Zhao, C. Jiang, K. J. Yu, Y. Zhong, D. Xu, J. Li, G. Fang, H. Du, J. Zhang, J. M. Park, Y. Huang, M. A. Alam, Y. Mei, and J. A. Rogers, Adv. Electron. Mater. **3**, 1700077 (2017).
[50]E. Song, Y. K. Lee, R. Li, J. Li, X. Jin, K. J. Yu, Z. Xie, H. Fang, Y. Zhong, H. Du, J. Zhang, G. Fang, Y. Kim, Y. Yoon, M. A. Alam, Y. Mei, Y. Huang, and J. A. Rogers, Adv. Funct. Mater. **28**, 1702284 (2017).
[51]X. Jin, C. Jiang, E. Song, H. Fang, J. A. Rogers, and M. A. Alam, IEEE Trans. Electron. Dev. **64**, 3443 (2017).
[52]R. Li, H. Cheng, Y. Su, S.-W. Hwang, L. Yin, H. Tao, M. A. Brenckle, D.-H. Kim, F. G. Omenetto, J. A. Rogers, and Y. Huang, Adv. Funct. Mater. **23**, 3106 (2013).
[53]A. Oehler and M. Tomozawa, J. Non-Cryst. Solids. **347**, 211 (2004).
[54]S. Nagai, J. Appl. Phys. **114**, 174302 (2013).
[55]K. M. Davis and M. Tomozawa, J. Non-Cryst. Solids. **185**, 203 (1995).
[56]H. Fang, K. J. Yu, C. Gloschat, Z. Yang, E. Song, C.-H. Chiang, J. Zhao, S. M. Won, S. Xu, M. Trumpis, Y. Zhong, S. W. Han, Y. Xue, D. Xu, S. W. Choi, G. Cauwenberghs, M. Kay, Y. Huang, J. Viventi, I. R. Efimov, and J. A. Rogers, Nat. Biomed. Eng. **1**(3), 0038 (2017).
[57]J. Shin, Y. Yan, W. Bai, Y. Xue, P. Gamble, L. Tian, I. Kandela, C. R. Haney, W. Spees, Y. Lee, M. Choi, J. Ko, H. Ryu, J.-K. Chang, M. Pezhouh, S.-K. Kang, S. M. Won, K. J. Yu, J. Zhao, Y. K. Lee, M. R. MacEwan, S.-K. Song, Y. Huang, W. Z. Ray, and J. A. Rogers, Nat. Biomed. Eng. **3**, 37 (2018).
[58]Y. K. Lee, K. J. Yu, E. Song, A. B. Farimani, F. Vitale, Z. Xie, Y. Yoon, Y. Kim, A. Richardson, H. Luan, Y. Wu, X. Xie, T. H. Lucas, K. Crawford, Y. Mei, X. Feng, Y. Huang, B. Litt, N. R. Aluru, L. Yin, and J. A. Rogers, ACS Nano **11**(12), 12562 (2017).
[59]J. Li, E. Song, C.-H. Chiang, K. J. Yu, J. Koo, H. Du, Y. Zhong, M. Hill, C. Wang, J. Zhang, Y. Chen, L. Tian, Y. Zhong, G. Fang, J. Viventi, and J. A. Rogers, Proc. Natl. Acad. Sci. U. S. A. **115**(41), E9542 (2018).
[60]J. Li, R. Li, H. Du, Y. Zhong, Y. Chen, K. Nan, S. M. Won, J. Zhang, Y. Huang, and J. A. Rogers, ACS Nano **13**, 660 (2019).